Supporting Information

Lüftner et al. 10.1073/pnas.1315716110

SI Text

Before the iterative procedure can be applied to the measured momentum maps, background intensity has to be subtracted from the angle-resolved photoemission spectroscopy (ARPES) data. To get rid of contributions arising from the diffuse substrate emission, the average polar angle Θ-intensity distribution of different azimuthal angles Φ where no molecular features are present is subtracted from the whole raw intensity data $I(\Theta, \Phi)$. Beside these subtractions for all measured orbitals, in the case of pentacene (5A)/Ag(110) there is a small amount of a second domain with molecules rotated 90° with respect to the main domain, which may impede the reconstruction procedure. The second domain may be seen for instance in the lowest un-occupied molecular orbital (LUMO) map at a k_y value of 1.4 Å^{-1} (Fig. 3C), but is also present in the other orbitals momentum maps. To handle this circumstance we rotate the corresponding experimental momentum map by 90° and subtract 10% of the so-rotated data from the original momentum map, getting rid of contributions from the minor domain.

The real-space resolution of the orbitals is given by the max-imum momentum value of the respective ARPES maps, which in turn is governed by the kinetic energy of the photoemitted electrons. Because the kinetic energies for the studied orbitals lie around 25 eV if photons of 30 eV are used, maximum k values around $k_{max} = 2.5$ Å^{-1} result. The resolution in real space would be therefore $\Delta x = \pi/k_{max} = 1.25$ Å. To obtain smoother orbital images, we expand the momentum space domain size to $\sim$17.5 Å^{-1} and set the data outside the measured $k_{max} = 2.5$ Å^{-1} to zero. Thereby, we can interpolate orbitals in real space on a denser grid with a spacing of $\pi/17.5 = 0.2$ Å. The data produced with these preparation steps were used as an input for the iter-ative procedure.

We relate the reconstructed orbitals to those measured with scanning tunneling microscopy (STM) (Fig. S1). As mentioned in the introduction, STM measurements probe the local density of states of the orbital at the position of the tip. Thus, no information on the phase of the wave function can be obtained in STM. In contrast, our ARPES-based reconstruction algorithm provides information about the phase, which we consider a major ad-vantage over orbital imaging in STM. As expected, there are clear similarities in the results of the two techniques, e.g., regarding the nodal structure of all orbitals (Fig. S1 A–H). However, there are also clear differences: Firstly, the lateral extensions of the orbi-tals in the STM measurements are larger than the reconstructed ones, most notably in the case of 5A (Fig. S1 A–D). We think that this is related to the fact that the probability density is de-tected at distances further away from the molecule, whereas in ARPES the orbital is cut in reciprocal space, which determines the size of the lobes. Secondly, Fig. S1 E and F illustrate the ambiguity of orbital images obtained from STM, arising from the influence of the tip. Thirdly, the ARPES-based reconstruction algorithm is not restricted to the LUMO and HOMO states of a molecule and should work independent of the chosen substrate.

In Fig. S2, which shows the same experimental data as Fig. 3 of the main text, the reconstructed orbitals are compared with 2D projections of the theoretical orbitals. These 2D projections $\phi(x,y)$ are obtained from the computed 3D orbitals, $\psi(x,y,z)$, in the following way:

$$\phi(x,y) = \int dz \; \psi(x,y,z) \cdot z e^{-c|z|}. \qquad \text{[S1]}$$

Here, the function $ze^{-c|z|}$ resembles the z dependence of a carbon p_z orbital where the parameter c is chosen accordingly.

For a further proof of the robustness of our method, Fig. S3 shows once again the iterative procedure, but now with a ran-domly k_x, k_y distributed phase as a starting point. The data and the color code used in this example are the same as for Fig. 2 of the main text. In Fig. S3A the first iteration of the procedure can be seen. Note the random distribution of the phase on the top left. After the first inverse Fourier transform, the so-obtained real-space intensity distribution, depicted in Fig. S3A (Right), shows no similarity to an actual molecular orbital, but resembles a random distribution. Arrow number 4 shows the last step that closes one iteration cycle, which consists of applying the newly obtained complex phase (Fig. S3A, Bottom Left) to the square root of the measured intensity $\sqrt{I}$ (Fig. S3B, Left). The real-space wave function obtained in the second cycle (Fig. S3B, Right) still looks like an irregular distribution. After 50 iterations (Fig. S3C) the real-space orbital is already close to the one ob-tained with the constant phase, and after the 250th iteration (Fig. S3D) the converged result is indeed the same as for reconstruction starting with a constant phase (Fig. 2). Performing several recon-structions with different initial random complex phase patterns leads to essentially identical results, apart from minor details, thereby maintaining the good agreement with the calculated density functional theory (DFT) orbitals.

The issue of orbital translation is illustrated in Fig. S4 for the second highest occupied molecular orbital (HOMO-1) orbital of 5A. Comparing the reconstructed orbital (Fig. S4A) with the Kohn–Sham orbital (Fig. S4C), the concordance between these two is not as good as for the other four orbitals. On closer in-spection, one may infer a better agreement if the reconstructed orbital is cyclically shifted in the direction indicated with the arrow. Such a shift may indeed result from the reconstruction algorithm, because a translation of the orbital in real space only leads to a constant phase factor in momentum space, due to the mathematical properties of Fourier transforms already men-tioned in point (ii) of the main text section, *How Can the Lost Phase Be Recovered?*. Therefore, the reconstruction algorithm cannot distinguish between a function $\phi(x,y)$ and the constant shifted function $\phi(x-R_x, y-R_y)$ multiplied with a phase factor $\exp(i\xi)$. To solve this ambiguity, we may choose to fix the posi-tion of the orbital's center in the middle of the confining box by applying inversion symmetry to the wave function during the iteration cycles. Doing so, we obtain the reconstructed orbital shown in Fig. S4B, whose shape is actually in good agreement with the DFT calculation.

Fig. S1. Comparison between the orbitals reconstructed iteratively from ARPES data and images of orbitals measured with STM. (*A* and *C*) STM images of the 5A LUMO and HOMO on NaCl/Cu(111) using a pentacene tip, taken from ref. 1. (*B* and *D*) The 5A LUMO and HOMO reconstructed from ARPES (*Upper*) and the corresponding Kohn–Sham orbital images (*Lower*). (*E* and *G*) STM images of the PTCDA LUMO and HOMO on Au(111) using a CO tip (*Left*) and a bare metal tip (*Right*). (*F* and *H*) PTCDA LUMO and HOMO reconstructed from ARPES (*Upper*) and the corresponding Kohn–Sham orbital images (*Lower*). *A* and *C* reprinted figure with permission from Repp J, Meyer G, Stojkovic SM, Gourdon A, Joachim C (2005) *Phys Rev Lett* 94(2):026803. Copyright 2005 by the American Physical Society, http://prl.aps.org/abstract/PRL/v94/i2/e026803.

1. Repp J, Meyer G, Stojković SM, Gourdon A, Joachim C (2005) Molecules on insulating films: Scanning-tunneling microscopy imaging of individual molecular orbitals. *Phys Rev Lett* 94(2): 026803.
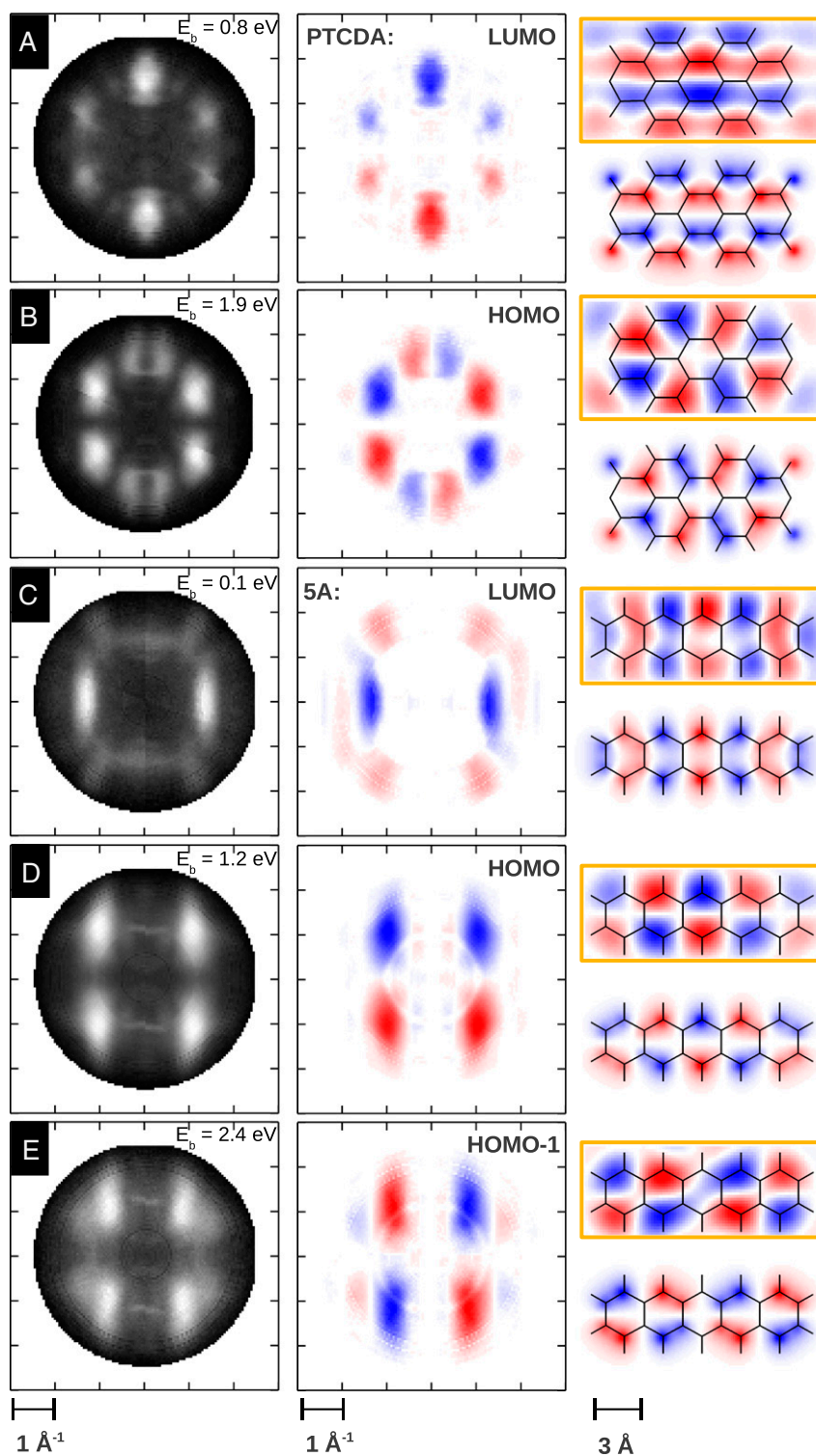
Fig. S2. Compilation of orbitals reconstructed from ARPES data in this work (same data as in Fig. 3 of the main text except for the theoretical orbital images). (*Left*) Experimental constant binding energy (CBE) ARPES maps of the PTCDA LUMO (*A*) and HOMO (*B*), and the pentacene LUMO (*C*), HOMO (*D*), and HOMO-1 (*E*). (*Center*) CBE maps with the recovered phase information. (*Right*) Reconstructed real-space orbitals (orange box) which are compared with corresponding 2D projections of Kohn–Sham orbital (without box) as explained in the text. The wave function confinement regions are 14.8 × 7.2 Å^2 and 14.8 × 5.4 Å^2 for PTCDA and pentacene, respectively.

Fig. S3. Illustration of the iterative wave function reconstruction algorithm with a random complex phase distribution as the starting point, using the example of the perylene-3,4,9,10-tetracarboxylic dianhydride (PTCDA) HOMO. Black isolines represent the square root of the measured intensities, whereas the color indicates the phase. (*A*) First iteration. (*B–D*) Reciprocal- (*Left*) and real-space (*Right*) picture of the wave function in the 2nd, 50th and 250th iterations, respectively. At the bottom of *D* we show the real part of the reconstructed wave function in *k* space and real space.
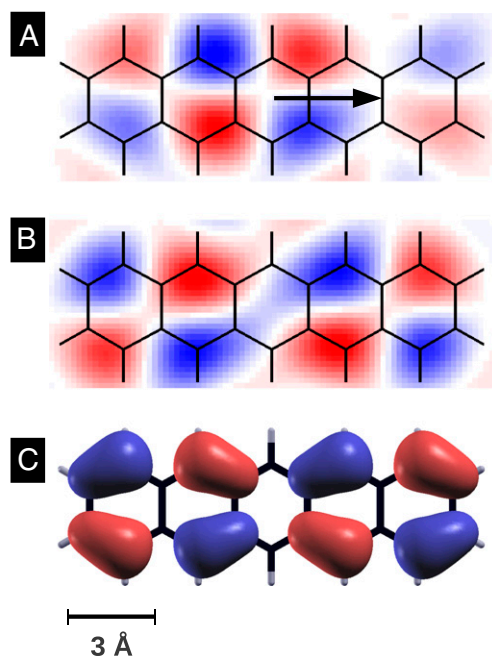
Fig. S4. Illustration of the cyclic translation that can result from incorrect spatial confinement. (*A*) Real-space reconstruction of the HOMO-1 orbital of 5A without any further constraints besides the spatial confinement of the orbital. (*B*) Real-space reconstruction of the HOMO-1 orbital applying inversion symmetry to the orbital during the iterative procedure. (*C*) Kohn–Sham orbital image of the HOMO-1 of 5A.